School of Geosciences Faculty and Staff
Publications

School of Geosciences

2-2020

Quantifying Rates of "Rifting while Drifting" in the Southern Gulf of California: The role of the Southern Baja California Microplate and its Eastern Boundary Zone

Paul J. Umhoefer
Northern Arizona University

C. Plattner
Ludwig-Maximilians Universität

Rocco Malservisi
University of South Florida, rocco@usf.edu

Quantifying rates of "rifting while drifting" in the southern Gulf of California: The role of the southern Baja California microplate and its eastern boundary zone

Paul J. Umhoefer[1],*, C. Plattner[2], and R. Malservisi[3]
[1]SCHOOL OF EARTH AND SUSTAINABILITY, NORTHERN ARIZONA UNIVERSITY, 624 S. KNOLES DRIVE, ASHURST BUILDING, ROOM A108, FLAGSTAFF, ARIZONA 86011, USA
[2]DEPARTMENT FÜR UMWELT- UND GEOWISSENSCHAFTEN, LUDWIG-MAXIMILIANS-UNIVERSITÄT MÜNCHEN, SEKTION GEOLOGIE, LUISENSTRASSE 37, 80333 MÜNCHEN, GERMANY
[3]SCHOOL OF GEOSCIENCES, UNIVERSITY OF SOUTH FLORIDA, 4202 E. FOWLER AVENUE, NES107, TAMPA, FLORIDA 33620, USA

ABSTRACT

The southern Baja California (Mexico) microplate has been rapidly moving away from the North America plate since ca. 12 Ma. This relative motion toward the northwest developed an oblique-divergent plate boundary that formed the Gulf of California. The rift-drift hypothesis postulates that when a continent ruptures and seafloor spreading commences, rifting on the plate margins ceases, and the margins start to drift, subside, and accumulate postrift sediments, eventually becoming a passive margin. In contrast to this hypothesis, the southern part of the Baja California microplate (BCM), and in particular its actively deforming eastern boundary zone, has continued significant rifting for millions of years after seafloor spreading initiated within the southern Gulf of California at 6–2.5 Ma. This is a process we call "rifting-while-drifting." Global positioning system (GPS)–based data collected from 1998 to 2011 show relative motion across the eastern boundary zone up to ~2–3.2 mm/yr with respect to a stable BCM. Furthermore, the velocity directions are compatible with normal faulting across the eastern boundary zone nearly perpendicular to the trend of the plate boundary at the latitude of La Paz and therefore a highly strain partitioned domain. North of 25°N latitude up to the Loreto area, there is a domain with no strain partitioning, and northwest-directed transtensional deformation dominates. From long-term geologic and paleoseismology studies, late Quaternary faulting rates are equal to or less than the GPS-derived rates, while geologic rates older than 1–2 Ma are commonly much higher. We suggest that the "rifting-while-drifting" process may be caused by the large topographic relief across the BCM margin, which created a significant gradient in gravitational potential energy that helps in driving continued relatively slow faulting. The relief was inherited from the much faster faulting of the BCM eastern boundary zone before plate motions largely localized along the modern transform–spreading centers in the axis of the Gulf of California. The low sediment flux from the small drainages and arid climate on the southern Baja California Peninsula result in the maintenance of underfilled to starved basins, and the relatively slow late Quaternary active faulting promotes continued topographic relief over millions of years.

INTRODUCTION

Divergent plate boundaries are one of the fundamental types of plate boundaries on Earth and the birthplace of oceans and marginal seas. It is generally accepted that the process required to form an ocean or marginal sea is a progression from rifting of a continent to continental rupture to formation of oceanic spreading centers, and finally development of passive margins along the former rift zones. The classic interpretation of the transition from rifting to seafloor spreading is the so-called "rift-to-drift" hypothesis, which postulates that once seafloor spreading and formation of oceanic crust commences, then rifting (faulting) across the margins of the plate boundary will cease (e.g., LePichon, 1968; Heezen, 1969).

In detail, however, the processes that occur at the critical transition from rifting and extreme thinning of continental lithosphere to complete rupture (breakup) of continental lithosphere and initiation of seafloor

spreading are poorly known. Part of the reason for this lack of knowledge is that there are few plate boundaries at which this process is young enough that the transition can be studied in an active system, while there are many ancient divergent plate margins where the early rift-to-drift record is buried under many kilometers of sediment along passive margins, or where it has not been explored in detail in the deep oceans. The central South Atlantic is an example of a location where the rift-to-drift hypothesis is largely borne out, but where a sag basin developed in the late stage of rifting above the older rift basins and faults (Mohriak and Leroy, 2013).

There are examples of deformation or magmatism that occurred after the initiation of seafloor spreading in a few ancient passive margins, but most of these are in the distal domain of the passive margin or near the continent-ocean boundary (or transition; Peron-Pinvidic et al., 2013). Contractional inversion structures have been documented off the Norwegian margin near the continent-ocean boundary (Masson et al., 1994). Magmatism occurred up to 15 m.y. after seafloor spreading started on the northern continent-ocean boundary of the Gulf of Aden (Lucazeau

Paul Umhoefer ⬤ http://orcid.org/0000-0002-6538-3335
*paul.umhoefer@nau.edu

et al., 2009), and across the distal domain of the Newfoundland margin as postrift sills (Schillington et al., 2008; Peron-Pinvidic et al., 2010).

The southern Gulf of California (Figs. 1 and 2) is one of the divergent plate boundaries in which the rifting to seafloor spreading features are relatively well exposed, though partly underwater. In the central to southern Gulf of California, seafloor spreading initiated along relatively short oceanic ridges and basins over the past 2.5–6 m.y. (Lonsdale, 1989; Lizarralde et al., 2007) after a short period of oblique rifting since ca. 12 Ma (Umhoefer, 2011), and following late Oligocene to middle Miocene extensional faulting to the east (Ferrari et al., 2002, 2013).

An interesting aspect of the southern Gulf of California plate boundary is that while rifting on the northeast side of the plate margin (along mainland Mexico) has ceased, in agreement with the rift-drift hypothesis, rifting along the southwest margin (or eastern boundary of the Baja California microplate [BCM]) has slowed, but continued after the 6–2.5 Ma initiation of seafloor spreading (Fig. 2). This active plate margin refutes the simple rift-drift hypothesis and represents the "rifting-while-drifting" phenomena documented in past observations and by the data presented herein. The rifting-while-drifting process along the southern BCM may be anomalous globally, or it may be common under certain circumstances but has remained undetected in many ancient plate margins.

In this study, we verified and quantified the strain rates across the southwestern plate margin of the Gulf of California from global positioning system (GPS) data over the past ~20 yr. We then compared the modern strain rates to faulting rates reported earlier at intermediate (late Quaternary) time scales from terrestrial and marine paleoseismology, and over longer time scales from structural geology and other data. This study builds on earlier studies based on recent earthquakes, which showed that the southwestern plate margin was active (Fletcher and Munguía, 2000; Munguía et al., 2006; Sumy et al., 2013). The active rates of faulting across the plate margin are uniformly lower than longer-term geologic rates, but they are about the same or faster than late Quaternary rates from paleoseismology. The active faulting across the plate margin presents a paradox: Why is faulting occurring at all a few million years after initiation of seafloor spreading, and how can such low faulting rates persist? We explored possible mechanisms that are promoting rifting while drifting millions of years after the initiation of seafloor spreading.

TECTONIC SETTING OF SOUTHERN GULF OF CALIFORNIA

The Gulf of California formed along an active oblique-divergent plate boundary since ca. 12 Ma (Lonsdale, 1989; Dorsey and Umhoefer, 2000),
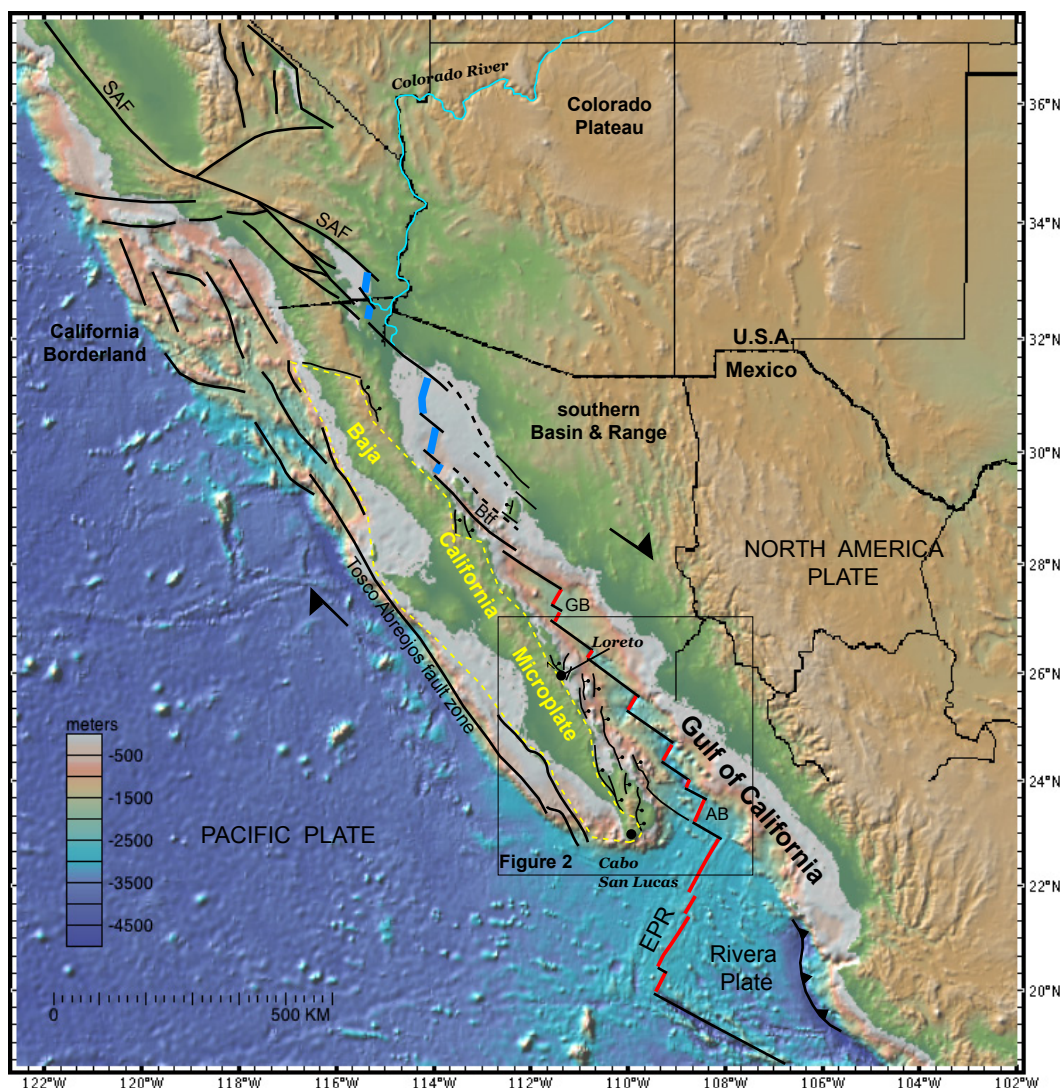

Figure 1. Tectonic map of the Gulf of California plate boundary. Main plate boundary: black lines are transform faults; red lines are spreading centers; blue lines are nascent or buried spreading centers. Only selected faults are shown outside the main boundary. SAF—San Andreas fault; GB—Guaymas basin; AB—Alarcón basin; EPR—East Pacific Rise; Btf—Ballenas transform fault.
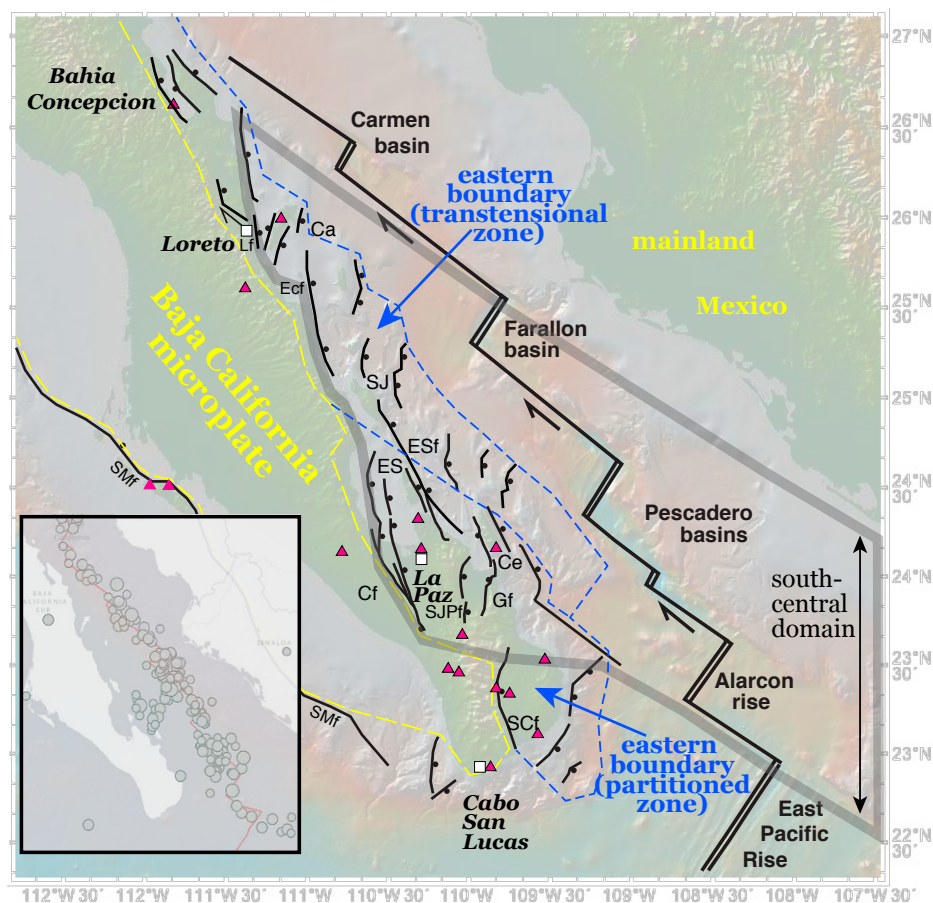
Figure 2. Map of the plate boundary in the southern Gulf of California showing the features of the main boundary, and the faults of the eastern boundary zone (see text for discussion) onshore and offshore of the southern Baja California Peninsula. Blue dashed lines denote the two structural domains of the eastern boundary zone. Red triangles are the global positioning system (GPS) sites of this study. Ca—Carmen Island; Ce—Cerralvo Island; Cf—Carrizal fault; Ecf—Escondido fault; ES—Espiritu Santo Island; ESf—Espiritu Santo fault; Gf—La Gata fault; Lf—Loreto fault; SCf—San Jose del Cabo fault; SJ—San Jose Island; SJPf—San Juan de los Planes fault; SMf—Santa Margarita–San Lazaro fault system. Inset map in lower left shows the magnitude >4.5 earthquakes from 2000 to 2019 from the U.S. Geological Survey earthquake website (https://earthquake.usgs.gov/).

following late Oligocene to middle Miocene extensional faulting mainly east of the plate boundary (Ferrari et al., 2002, 2013). The active plate boundary in the Gulf of California includes two main belts: the main axial system in the gulf itself and an active fault system along the southwestern gulf (Fletcher and Munguía, 2000; Busch et al., 2011; Plattner et al., 2007). The gulf-axis system is the focus of the majority of relative plate motion (Plattner et al., 2007) through an array of en echelon right-stepping transform faults and oceanic spreading centers (Fig. 1). The gulf-margin fault system is the eastern boundary of the BCM and the focus of this study in the southern Gulf of California. The portion of the older plate boundary now east of the gulf-axis system is virtually inactive (Fig. 2; Goff et al., 1987; Sumy et al., 2013; Bennett et al., 2013). A small portion of the plate boundary is active on faults of the Tosco-Abreojos fault system west of the BCM (Dixon et al., 2000; Brothers et al., 2012).

The rift escarpment along the eastern side of the Baja California Peninsula (and BCM) is bounded by mainly normal faults; the escarpment dies out to the south along the Carrizal fault west of La Paz, and then faulting jumps to the southeast to the San Jose del Cabo fault (Fig. 2). The normal faults near the escarpment in the gulf-margin fault system north of La Paz Bay to Loreto and Bahia Concepcion are linked, and they step southeast to a belt of inferred oblique- and strike-slip faults offshore, based on their more northwesterly strike. These faults are interpreted as a zone of transtensional faults and basins (e.g., Umhoefer et al., 2007) that lies largely along the narrow offshore shelf from the Loreto area to the Alarcón Rise. The overall gulf-margin fault system or eastern boundary zone of the BCM forms a north-tapering wedge in map view that is ~100 km wide in the south and narrows and dies out to the north near Bahia

Concepcion (Fig. 2). Evidence presented and summarized here suggests that the eastern boundary zone has two distinct domains. Recent seismicity supports at least some of this transtensional belt being active (Fig. 2). Based on a seismic refraction line, the BCM crustal thickness rapidly thins under the eastern boundary zone from ~30 km under the rift escarpment to 15 km at the eastern edge of the boundary zone (Brothers et al., 2012).

The southern gulf axis is well defined by earthquakes and bathymetry (Fig. 2). The northern East Pacific Rise has been active since 4.5 Ma, and the Maria Magdalena Rise (SE of the north end of the East Pacific Rise) was active from 5.5 to 4.5 Ma along its southeastern flank (Lonsdale, 1991). The Alarcón Rise has been active since 3.5 Ma (DeMets, 1995), with an early history of underplating from ca. 3.5 to 2.4 Ma, followed by full seafloor spreading (Sutherland, et al., 2012). The Pescadero and Farallon spreading centers are basins of 2–3 km depth that appear to have been active since 2–1 Ma based on the width of the deep oceanic crust (Fig. 1). The Alarcón to Farallon rift domains, including the eastern boundary zone of BCM, form the south-central domain of Lizarralde et al. (2007; see also Fig. 2 herein).

GPS DATA ANALYSIS

Methods

The Baja California Peninsula hosts a GPS campaign network that was installed and maintained by the University of Miami (USA), Ludwig-Maximilians University of Munich (Germany), University of South Florida (USA), and Centro de Investigacion Cientifica y Education Superior de

Ensenada (CICESE, Mexico). The local network in southern Baja California consists of 16 campaign stations (Fig. 2) from which data were collected in 1996 (for CABO and CONC only), 1998, 2001, 2004, 2006, and 2011, with 2–5 d of continuous 24 h data observation during each campaign. In addition to the local network, we included five of our campaign stations in northern Baja California for an updated calculation of the stable BCM Euler vector (Plattner et al., 2007) with respect to the IGb08 reference frame (Rebischung et al., 2012). We did not include data from central Baja California due to significant deformation from interseismic strain accumulation and/or postseismic deformation associated with the Mw 6.9 Ballenas transform fault (Fig. 1) earthquake of 2009 (Plattner et al., 2015). We also included data from permanent GPS station LPAZ (with data from 2004 to 2011, avoiding data after 2012 for possible technical problems) in southern Baja California, operated by the Instituto Nacional de Estadística y Geografía (Mexico). We did not include the continuous sites IPAZ and MSD1 in southern Baja California, because, for both, we observed velocities that were out of realistic bounds, indicating that both sites have possible problems with monumentation or are installed in an area affected by deformation not associated with tectonic processes.

GPS data were processed at the University of South Florida using GYPSY/OASIS II, Release 6.4, software and non-net-rotation satellite orbit and clock files provided by the Jet Propulsion Laboratory (JPL; Zumberge et al., 1997). The analysis followed the description of Wetmore et al. (2019) and Malservisi et al. (2015), with the daily solutions aligned to IGb08 (Rebischung et al., 2012). At the processing time (December, 2018), the JPL reprocessing of the orbits for ITRF2014 did not go earlier than 2000. To maintain a uniform processing and reference frame throughout the full period of observations of the southern Baja California network, we decided to align our solution to IGb08. A test with stations from a different network showed that the effects of using IGb08 instead of ITRF2014 for old campaign data were within the noise of our uncertainties. The daily position time series were used in a weighted linear least squares

regression to calculate sites velocities. To estimate velocity uncertainties, we used the methods of Mao et al. (1999) for campaign observation and the Allan variance of velocity (Hackl et al., 2011). Time series of the GPS positions with time are included in the GSA Data Repository Item[1].

The use of campaign GPS data to analyze deformation of the order of a few millimeters per year does not consider the transient effects that could be identified through the use of continuous time series, both due to tectonic deformation (e.g., Wernicke and Davis, 2010) or hydrological effects (e.g., Amos et al., 2014; Chamoli et al., 2014; Fu et al., 2015). Fortunately, our time series were so long that many of these effects would be averaged out, and the decal length tectonic signal was visible in our data set. Of course, our velocity field should be interpreted as an average value for the studied period (and thus cannot take into account long-term geodynamic effects similar to those suggested by Friedrich et al., 2004, for the Basin and Range). The strong agreement between the geologic and geodetic observations (Table 1) discussed in this paper suggests that the length of our time series was long enough to observe the underlying geological processes happening in the southern Baja California region.

The IGb08 computed velocity field was transformed in a local reference frame through the use of an Euler vector describing Baja California rigid plate/block rotation. Following Plattner et al. (2007), we calculated the Euler vector describing the motion of the full BCM with respect to IGb08 (Table 2). The differences between the observed velocity field and the velocity field computed using the Euler vector provide the motion with respect to the reference frame defined by the motion of a rigid BCM (Data Repository Fig. DR1 and Table DR1). The resulting velocity field confirms the observations by Plattner et al. (2007), i.e., that the motion of the south Baja California sites with respect to a reference defined

[1]GSA Data Repository Item 2020115, GPS velocities in tables (data) and maps (vectors), is available at http://www.geosociety.org/datarepository/2020, or on request from editing@geosociety.org.

TABLE 1. VELOCITY OF GLOBAL POSITIONING SYSTEM (GPS) STATIONS IN THE ITRF08 REFERENCE FRAME AND RESIDUAL MOTION WITH RESPECT TO SOUTHERN BAJA CALIFORNIA REFERENCE FRAME

Site ID	Long (°E)	Lat (°N)	ITRF08				Residual to southern BCM		
			Ve (mm yr^{-1})	$1\sigma\ Ve$ (mm yr^{-1})	Vn (mm yr^{-1})	$1\sigma\ Vn$ (mm yr^{-1})	Rate (mm yr^{-1})	1σ Rate (mm yr^{-1})	Azimuth (°)
AGUA*	−111.30	25.59	−48.0	0.4	20.9	0.3	0.5	0.3	168
ANCN	−110.03	23.74	−49.5	0.5	20.8	0.3	0.2	0.4	−142
blnd	−110.31	24.33	−48.0	0.4	21.5	0.2	1.1	0.3	65
BURR	−110.07	23.52	−49.2	0.3	21.2	0.2	0.4	0.3	60
CABO*	−109.86	22.92	−50.1	0.4	20.4	0.2	0.5	0.5	−160
cadg*	−116.32	31.36	−42.9	0.4	21.2	0.3	2.4	0.4	145
CARD*	−110.78	24.15	−48.6	0.4	21.4	0.3	0.5	0.3	75
colo*	−116.21	31.10	−43.1	0.4	22.2	0.4	1.6	0.5	124
conc*	−111.81	26.62	−45.8	0.3	21.2	0.2	1.6	0.4	104
ecer	−109.81	24.18	−47.6	0.4	22.3	0.3	2.0	0.4	44
emar	−111.90	24.51	−49.5	0.5	20.8	0.2	0.9	0.5	−152
emir	−109.74	23.37	−49.6	0.6	20.8	0.4	0.1	0.5	129
lpaz	−110.32	24.14	−48.6	0.3	21.3	0.3	0.5	0.3	39
melr*	−115.74	30.98	−43.5	1.0	21.9	0.9	1.5	1.0	137
rive	−109.53	23.55	−48.6	0.6	20.9	0.4	0.8	0.6	82
sais*	−116.22	31.19	−42.8	0.4	21.6	0.3	2.1	0.4	134
slre*	−116.16	31.26	−43.0	0.5	20.8	0.3	2.6	0.5	150
TOSA*	−110.13	23.54	−49.2	0.5	21.4	0.2	0.5	0.5	38
wcar	−111.16	26.02	−45.5	1.1	19.1	0.4	3.2	0.9	136
wmar	−111.98	24.51	−49.0	0.7	21.3	0.7	0.3	0.7	165
WMIR	−109.82	23.39	−49.5	1.2	20.6	0.5	0.3	1.1	151
zaca	−109.58	23.08	−49.6	1.1	20.6	0.7	0.3	0.9	128

Note: Sites used for southern Baja California reference frame are capitalized. For residual velocities, see Data Repository Table DR1 (text footnote 1). Uncertainties are 1σ. *Ve*—Velocity east; *Vn*—Velocity north.
*Sites used for Baja California microplate (BCM) reference frame by Plattner et al. (2007).

assuming the full BCM to be a single rigid block indicates a northward component well outside the uncertainties, suggesting a convergence rate of ~3 mm/yr between the northern and southern GPS networks. This observation raises the question: Does a local reference frame for only the southern BCM provide a better fit to study the local deformation of the southern Baja California Peninsula? A local reference frame would remove this northward component of motion (Data Repository Fig. DR1) and would allow better constraints on the local deformation rates.

Using the seven sites indicated in capital letters in Table 1, we computed a new Euler vector describing the motion of a southern Baja California rigid block with respect to IGb08. A Fisher test (Stein and Gordon, 1984) indicated that the separation of the full BCM into two different reference frames, one for the north and one for the south, improves the description of the rigid block motion with a 95% confidence. We decided not to include the station CONC in the calculation of the reference frame, yielding a significantly better fit and the possibility of active faults along the west side of Bahia Conception (Ledesma-Vazquez and Johnson, 2001) causing strain accumulation to bias the plate velocity. The best-fitting Euler vector for the motion of southern Baja California has a reduced χ^2 misfit of 0.3, indicating a very good model fit and suggesting that GPS velocity uncertainties are overestimated. This overestimation of the uncertainties by the analysis of Mao et al. (1999) was already observed in the past (e.g., Hackl et al., 2011). In order to obtain more reasonable uncertainties for our sites, we followed the suggestion of Bennett et al. (2003), and we scaled the uncertainties associated with the observed GPS velocities until the reduced χ^2 associated with the calculation of the southern Baja California Euler vector as of the order of 1.0 (scaling the uncertainties by multiplying by a factor of 0.55). Note that this method will not allow us to use χ^2 values to do any statistical analysis about the significance of the fit. Table 1 reports the observed velocities with the scaled uncertainties. We note that even with this reduction of the uncertainties associated with the observed velocities, all the uncertainties for the sites used for the Euler vector calculation are still larger than the formal error computed assuming a white noise. Given the length of our time series, a white noise error would be in the range of 0.05–0.20 mm/yr.

Figure 3 shows the resulting GPS velocity field with respect to the southern BCM. The main differences for this velocity field, with respect to the one referenced to the BCM (Data Repository Fig. DR1), are that the azimuths of the reference station velocities in a southern BCM reference frame do not have a consistent northward direction but seem to be randomly directed, and the residuals of the seven sites used for the calculation of the new reference are all within the scaled uncertainties (average residual is 0.4 mm/yr). This suggests that the selected network describes the motion of a rigid block and provides a better representation of the rigid block motion for the southern BCM. Furthermore, the direction of the velocities of the sites not used to compute the reference frame are now very consistent with a motion perpendicular to the strike of known normal faults in the region. In the following discussion, we refer to the velocity uncertainties at 95% confidence. Formal uncertainties associated with the inversion of the Euler vector are also accounted for in the given velocity field.

Results

Across La Paz Bay and toward Espiritu Santo and Cerralvo Islands, we observed significant motion relative to the southern BCM, with rates increasing from west to east (LPAZ 0.5 ± 1.4 mm/yr, BLND 1.1 ± 0.6mm/yr, and ECER 2.0 ± 0.8 mm/yr; Fig. 4, profile A-A′). The 2 mm/yr is a minimum, because our GPS network cannot account for the possibly significant motion on the eastern Cerralvo fault, which had

TABLE 2. BAJA CALIFORNIA AND NORTH AMERICA EULER VECTORS

Rotation pole*						
Long. (°E)	Lat. (°N)	Omega[†] (deg m.y.⁻¹)	Max*	Min*	Azimuth[§] (°)	χ/d.o.f.
Baja California microplate (BCM), IGb08						
108.58	−63.50	0.6466 ± 0.0186	1.6	0.2	−56.2	1.44
Southern Baja California microplate (SBCM), IGb08						
114.70	−64.72	0.6273 ± 0.0440	4.8	0.1	−57.5	1.00
North America, ITRF08 (Kreemer et al., 2018)						
−86.03	−2.28	0.2010 ± 0.0009	0.3	0.3	−0.2	
BCM, North America						
−77.41	49.61	0.7493 ± 0.0216	1.2	0.2	63.4	
SBCM, North America[#]						
−74.17	50.48	0.7249 ± 0.0537	3.0	0.1	59.8	

Note: The first plate rotates counterclockwise relative to the second plate around the stated rotation pole. χ/d.o.f.— reduced Chi² misfit (i.e., Chi² divided by the degrees of freedom).

*Length in degrees of the semimajor axes (sig maj) and semiminor axes (sig min) of the 1σ pole error ellipse. Both axes were derived from a two-dimensional error distribution.

[†]Omega (10^{-3} rads m.y.⁻¹): omegaX = −1.9534994; omegaY = 4.2473913; omegaZ = −9.8997597. Covariance matrix (10^{-6} rads m.y.⁻¹): xx = 0.1473047; xy = 0.3956792; xz = −0.1847295; yy = 1.0663476; yz = −0.4976451; zz = 0.2326153.

[§]Azimuth of the semimajor ellipse axis in degrees clockwise from north.

[#]Angular velocity of the southern Baja California microplate (SBCM) is relative to ITRF08 in Cartesian coordinates with covariance matrix where the x, y, and z axes are parallel to (0°N, 0°E), (0°N, 90°E), and (90°N), respectively.
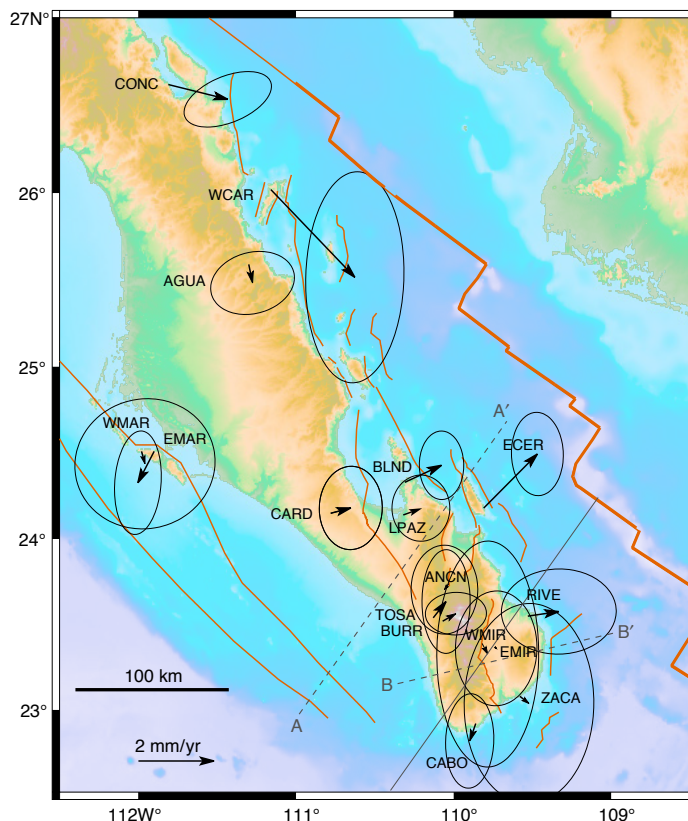

Figure 3. Global positioning system (GPS) velocity field and uncertainties (95% confidence) relative to southern Baja California microplate reference frame (SBCM; Euler pole IGb08 in Table 2). Profiles A-A′ and B-B′ were used for differential velocities (Fig. 4) and topographic gradient (Fig. 6).

two moderate earthquakes in 1969 (5.6, 5.0 M; Fletcher and Munguía, 2000), and significant seismicity since 2000 to the northeast of Cerralvo island and west of the gulf-axis boundary (Fig. 2; Sumy et al., 2013). The velocity azimuths are directed east to northeast, almost perpendicular to the northern Carrizal, San Juan de los Planes, and Cerralvo faults (Fig. 3).

We refrained from fault strain accumulation modeling due to the paucity of GPS stations within the network with respect to the number of active faults in the area, which make it impossible to establish a partitioning among the different faults. However, to provide some estimate on relative motions, we first calculated the approximately fault-perpendicular (assuming normal faulting) component of GPS velocities from stations across and close to the local fault network (Fig. 4; Data Repository Table DR2), and we derived differential rates between each pair of GPS stations across the faults. The fault-perpendicular component of the uncertainty ellipse was thereby calculated following Hackl et al. (2013), and for differential velocities, we assumed uncertainties to add in quadrature (Fig. 4A). As the differential velocities varied depending on the chosen pair of GPS stations, we calculated the average rates and uncertainties in order to allow better comparison with geological rates. Where multiple stations (>2) were located on each side of the fault, we applied the bootstrapping method (Efron, 1979) with 1000 data samples to get a more robust estimate of the deformation rate.

Figure 4A shows the GPS velocity component parallel to transect A-A′, which is oriented nearly perpendicular to the plate boundary (Fig. 3). The maximum differential velocity across the southern BCM's eastern margin is 2.5 ± 1.1 mm/yr (CABO – ECER), with more moderate rates of 1.6 ± 1.1 mm/yr (CARD – ECER) across the northern Cabo block. Across the Carrizal fault, we observed 0 ± 1.0 mm/yr (CARD – LPAZ) and 0.5 ± 1.1 mm/yr (CARD – BLND), averaging to a value of 0.2–0.3 ± 1.1 mm/yr. Across the zone of faulting that includes the San Juan de los Planes fault and its offshore extensions to the north, the Espiritu Santa fault and the La Gata fault (and its offshore extension on the west side of Cerralvo Island), we observed 1.6 ± 1.0 mm/yr (LPAZ – ECER) and 1.1 ± 1.1 mm/yr (BLND – ECER) in the north, and 2.2 ± 1.2 mm/yr (ANCN – ECER), 1.4 ± 1.3 mm/yr (TOSA – ECER), and 1.6 ± 1.0 mm/yr (BURR – ECER) in the south. Using these five differential velocities in the bootstrapping method to derive the mean velocity, we obtained 1.6 ± 1.1 mm/yr. Moderate changes to the profile azimuth caused only minor changes in the differential velocities, mainly reducing the rates seen between ECER and the onshore sites (e.g., by up to 0.2 mm/yr for the azimuth of profile B-B′).

East of the San Jose del Cabo fault, all GPS velocities on the Baja California Peninsula are insignificant (Fig. 3). Nevertheless, we interpreted the potential deformation rate, which is higher at site RIVE (0.8 ± 1.2 mm/yr) than at EMIR (0.1 ± 1.0 mm/yr) and ZACA (0.3 ± 1.8 mm/yr). The azimuth of the velocity at RIVE is oriented nearly perpendicular to the adjacent, northern San Jose del Cabo fault (82°), but the velocity azimuths of RIVE, ZACA, and CABO also point toward the deep basins in the Gulf of California (Fig. 3). Figure 4B shows the potential increase in velocity across the San Jose del Cabo fault, from southwest to northeast, using the parallel velocity component from transect B-B′ (Fig. 3), which strikes approximately perpendicular to the San Jose del Cabo fault. We observed a total differential velocity of 1.1 ± 1.4 mm/yr between CABO and RIVE. Across the southern San Jose del Cabo fault, we observed 0.5 ± 1.8 mm/yr (CABO – ZACA) and 0.3 ± 1.6 mm/yr (CABO – EMIR). Across the southeastern Cabo basin, we observed 0.6 ± 1.7 mm/yr (ZACA – RIVE) and 0.8 ± 1.5 mm/yr (EMIR – RIVE). Using the differential velocities and uncertainties across the San Jose del Cabo fault (using sites CABO, WMIR, TOSA, BURR, and ANCN on one side and ZACA, EMIR, and RIVE on the other) in the bootstrapping method, we derived
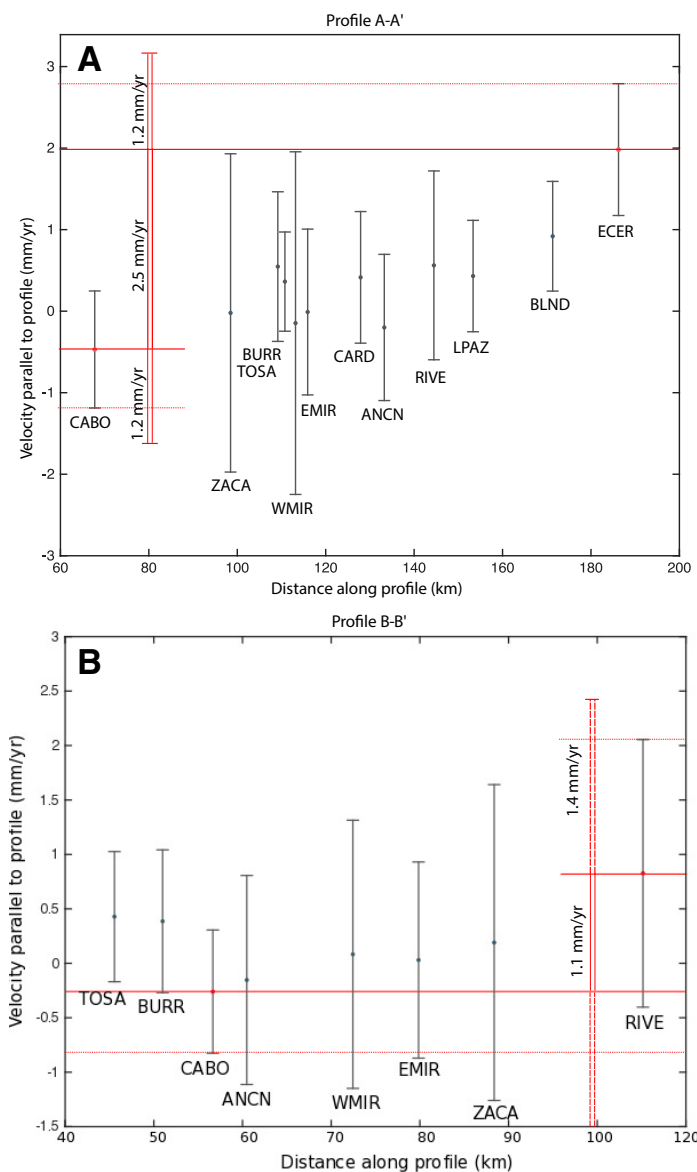
Figure 4. Global positioning system (GPS) velocity and uncertainty (95% confidence) components parallel to transects A-A′ and B-B′ (shown in Fig. 3). Examples for deriving the differential rate and uncertainty (considering error summation) are given (in red) for the GPS stations CABO and ECER (in A) and CABO and RIVE (in B).

a mean differential velocity of 0.4 ± 1.4 mm/yr. Excluding the sites in the near-field of the fault (EMIR and WMIR), the rate rises to 0.5 ± 1.5 mm/yr. For a modified transect azimuth (e.g., A-A′), the rates differ only slightly (Fig. 4A; mean differential velocity of the sites listed above is 0.4 ± 1.5 mm/yr but shows a greater extension rate for CABO – EMIR of 0.5 ± 1.5).

North of the La Paz–Cabo area in the Loreto domain, we found significant relative motion with respect to the southern BCM on the peninsula west of Bahia Concepcion (CONC = 1.6 ± 0.8 mm/yr) and on Carmen Island (WCAR = 3.2 ± 1.8 mm/yr). Both velocity azimuths were directed southeast (CONC toward 104°; WCAR toward 136°), nearly perpendicular to the strike of normal faults between the peninsula and Carmen Island (Fig. 3; Nava-Sanchez et al., 2001). Using the parallel velocity component

of a transect connecting the two GPS stations, which is again nearly perpendicular to the normal faults offshore Carmen Island, the differential velocity was 1.8 ± 1.8 mm/yr. The relative motion between the site on Carmen Island (WCAR) and a nearby site within the rigid southern BCM (AGUA) was 3.0 ± 1.0 mm/yr. Note that the direction of motion on Carmen Island relative to the southern BCM is nearly parallel to the adjacent transform fault and therefore the main azimuth of relative plate motion between the BCM and North America.

For completeness of the velocity field analysis, we included GPS sites on east and west Santa Margarita Island (EMAR, WMAR) along the west side of the Baja California Peninsula, although their velocities were less constrained because observations in 2011 (and 2001 for EMAR) were missing due to logistical problems in accessing the location. The GPS velocities were null within the uncertainties (EMAR = 0.9 ± 1.0 mm/yr to −152°; WMAR = 0.3 ± 1.4 mm/yr to 164°), but, again, the velocity azimuths were nearly perpendicular to the Santa Margarita–San Lazaro fault system (Fig. 2). Using the azimuth of profile A-A′ (Fig. 3), we obtained extension rated of 0.6 ± 1.7 mm/yr (WMAR – CARD), 1.3 ± 1.3 mm/yr (EMAR – CARD), 0.2 ± 1.7 mm/yr (WMAR – CABO), and 0.5 ± 1.3 mm/yr (EMAR – CABO; Fig. 4C). The differential velocity of the profile-perpendicular component between these stations is less than 0.2 mm/yr and well within the uncertainty, possibly implying that relative motion between the southern BCM and the Pacific plate by dextral slip entirely occurs on the Tosco-Abreojos fault west of the peninsula.

Using the stable North America (NOAM) reference frame with respect to IGS08 from Kreemer et al. (2018), we calculated the southern Baja California velocity field with respect to stable North America (Data Repository Table DR1) as well as the expected relative motion between the BCM and the southern BCM with respect to a stable North America at the seafloor spreading centers in the southern Gulf of California (49.8 ± 0.4 mm/yr to 306° for Alarcón basin relative to the southern BCM; Table 3; Data Repository Fig. DR2). The two relative motion estimates overlap within the 95% confidence interval. We can observe a consistently faster motion (~1 mm/yr) for the southern BCM–NOAM pair with respect to the velocity of the BCM–NOAM pair. In general, our BCM–NOAM and southern BCM–NOAM values agree with global plate motion models (Table 3). Specifically, our southern BCM–NOAM velocity is ~1.5 mm/yr faster than the Baja California–North America rates from geodetic plate motion model GSRM2.1 (Kreemer et al., 2014) and ~2 mm/yr faster than the 3 m.y. average geological rate in the Gulf of California from Nuvel-1A (DeMets et al., 1990, 1994). In contrast, our southern BCM–NOAM rates are ~2–2.5 mm/yr slower than Pacific–North America plate motion from MORVEL (DeMets et al., 2010), confirming deformation between the Pacific and southern Baja California offshore west of the peninsula.

PALEOSEISMOLOGY AND LONGER-TERM GEOLOGIC FAULTING RATES

Recent studies have documented late Quaternary faulting within the eastern boundary zone of the BCM from near Loreto to the Los Cabos area. In the north, numerous active faults have been documented in the Loreto area. Onshore, the northern Loreto fault and Escondido fault (~20 km south of the city of Loreto; Fig. 2) have evidence for late Quaternary faulting. The northern Loreto fault has 30 m of Quaternary offset and a faulting rate of ~0.2 mm/yr based on analysis of fault scarps that cut Quaternary deposits (Mayer and Vincent, 1999). Modern activity on the Escondido fault is based on local faulting of Quaternary deposits, Quaternary gravels in the fault zone with marine shells >100 m above the hanging wall basin, which lies near sea level in the central part of the fault zone, and the general geomorphology, characterized by a steep and straight footwall escarpment with peaks up to 1400 m high about 2 km from the fault and very short drainages (Umhoefer et al., 2002). Along the eastern margin of the Loreto basin, marine terraces were uplifted 10–20 m since ca. 120 ka, suggesting an active fault along the coastline on the east side of the steep Sierra Microondas (Mayer and Vincent, 1999; Umhoefer et al., 2002). Based on shallow geophysics, Quaternary faulting forms a graben offshore between Loreto and Carmen Island (Nava-Sanchez et al., 2001) and is suggested on both sides of Carmen Island based on uplifted marine terraces (Macy, 2005) and a large decapitated Pliocene-age delta now 60 m above sea level across the central part of the island (Johnson et al., 2016). Preliminary paleomagnetic data (Macy, 2005) support the conclusion from structural data that Carmen Island rotated clockwise ~30°–40°, probably in the Pliocene to Quaternary (Umhoefer et al., 2002).

The Carrizal and Centenario faults form the western border fault of the gulf-margin fault system west of La Paz (Fig. 2). Geologic and geomorphic mapping, optically stimulated luminescence (OSL) geochronology, and paleoseismic investigations onshore, seismic CHIRP profiling offshore, and analysis of uplifted marine terraces in the footwall of the offshore Carrizal fault quantify late Pleistocene–Holocene faulting along the Carrizal fault (Umhoefer et al., 2014). The onshore Carrizal fault has ruptured with up to ~1–2 m of vertical displacement per event, and up to three events are documented in trenches since 22 ka. Based on uplifted marine terraces along the western side of La Paz Bay, the fault shows offset rates of 0.1–0.2 mm/yr since 128 ka, and possibly since marine oxygen-isotope stage (MIS) 11 terraces (420 ka; Umhoefer et al., 2014).

Detailed geologic and geomorphic mapping along the onshore San Juan de los Planes (Fig. 2) and Saltito fault zones, and a CHIRP survey up to ~10 km offshore gave faulting rates east of La Paz (Coyan et al., 2013). The results suggest rates of active faulting of 0.25–1 mm/yr across

TABLE 3. RELATIVE MOTION AT SPREADING CENTERS IN THE SOUTHERN GULF OF CALIFORNIA FROM PLATE MOTION MODELS AND THIS STUDY

Location	Long (°E)	Lat (°N)	NUVEL-1A PAC-NOAM		GSRM 2.1 BC-NOAM		Morvel PAC-NOAM		This study BCM-NOAM		This study SBCM-NOAM	
			Rate (mm yr⁻¹)	Azi (°)	Rate (mm yr⁻¹)	Azi (°)	Rate (mm yr⁻¹)	Azi (°)	Rate (mm yr⁻¹)	Azi* (°)	Rate (mm yr⁻¹)	Azi* (°)
East Pacific Rise	−108.39	22.46	48.5	305	49.2	304	52.7 ± 1.8	308	49.7 ± 0.5	304	50.5 ± 0.4	305
Alarcon basin	−108.45	23.41	47.6	306	48.3	305	51.9 ± 1.8	309	48.9 ± 0.5	305	49.8 ± 0.4	306
South Pescadero basins	−108.83	23.99	47.3	306	48.0	305	51.6 ± 1.8	310	48.5 ± 0.5	306	49.4 ± 0.4	306
Pescadero basin	−109.15	24.51	47.0	307	47.6	306	51.4 ± 1.8	310	48.2 ± 0.5	306	49.1 ± 0.4	307
Farallon basin	−109.88	25.45	46.6	308	47.2	307	51.1 ± 1.8	312	47.7 ± 0.5	307	48.7 ± 0.5	308
Carmen basin	−110.76	26.40	46.3	310	46.9	309	50.9 ± 1.8	313	47.4 ± 0.5	309	48.5 ± 0.6	309
Guaymas basin	−111.48	27.33	46.0	311	46.5	310	50.6 ± 1.8	314	47.0 ± 0.5	310	48.1 ± 0.6	310

Note: Uncertainties are at 95% confidence. PAC—Pacific; NOAM—North America; BCM—Baja California microplate; SBCM—southern Baja California microplate; Azi—azimuth. NUVEL-1A—DeMets et al. (1990, 1994); GSRM 2.1—Kreemer et al. (2014); MORVEL—DeMets et al. (2010).
*The uncertainty of the azimuth is less than or equal to one degree for all estimates.

the San Juan de los Planes fault system, with ~2 m of vertical offset per event and with recurrence between 2 and 12 k.y., broadly similar to the Carrizal fault system. The offshore CHIRP survey suggests that the La Gata fault on the east side of San Juan de los Planes basin, and its extension west of Cerralvo Island, is a more active fault (Fig. 2), but the rates have not been quantified.

Geologic long-term (10^6 yr) faulting rates from Loreto to the Los Cabos area are similar to the late Quaternary rates on some faults, and higher on others. The overall faulting rate across the Gulf of California since ca. 12 Ma is 35–40 mm/yr (Lizarralde et al., 2007), while the current rate between the southern BCM and North America is ~50 mm/yr across the Alarcón basin, which has been active since 3.5–2.4 Ma. If there was a symmetric plate boundary before the onset of the Alarcón basin spreading ridge, then faulting rates across the southwestern Gulf of California margin were ~15–20 mm/yr, i.e., much higher than late Quaternary and present rates. The style, depth, and estimated history of basins across the southern Gulf of California along a Alarcón basin transect as imaged in seismic reflection data support these conclusions for the approximate rates of faulting (Sutherland et al., 2012).

Long-term faulting rates (shown in Fig. 5) in the Loreto basin were calculated with a short pulse of rapid faulting of 6–8 mm/yr at 2.4 Ma, and slower rates of 0.4 mm/yr before 2.46 Ma and after 2.36 Ma (Dorsey and Umhoefer, 2000). Across La Paz Bay, rates of 0.3 mm/yr were estimated based on offset of the Comondu Group by ~3.5 km on the Carrizal fault in simple cross sections from Espiritu Island to the rift escarpment (Puchalski, 2002). Long-term faulting rates across the San José del Cabo fault of 0.4–0.7 mm/yr are based on apatite fission-track thermochronology

(Fletcher et al., 2000) of the footwall of the fault. Busch et al. (2011) showed that gravity surveys suggested a more complex faulting history within the basin that would imply lower rates of faulting on the San José del Cabo fault for much of its history, but a similar overall rate across the basin.

DISCUSSION AND CONCLUSIONS

In this section, we explore the current rates and directions of faulting in the eastern boundary zone of the BCM, which differ substantially from north to south along the margin. We also summarize how the current faulting compares to that through the history of the plate boundary in the southern Gulf of California. Finally, we return to the question of why rifting while drifting is occurring in the SW part of the eastern boundary zone of the BCM 6–3 m.y. after the initiation of seafloor spreading.

Current Strain Behavior along Baja California Sur

The eastern boundary zone of the southern BCM shows much different behavior in the north near Loreto versus in the south in the La Paz to Cabo San Lucas area. The northern GPS site on Carmen Island (WCAR; Fig. 3) moves away from the BCM parallel to the transform fault, and thus subparallel to modern plate motion of the BCM relative to North America, while the GPS site in Bahia Concepcion at the margin of the BCM (CONC; Fig. 3) moves at an intermediate direction away from the BCM and within 30° of the transform fault. This suggests that the transtensional zone north of 25°N and offshore of Loreto is largely hard-linked
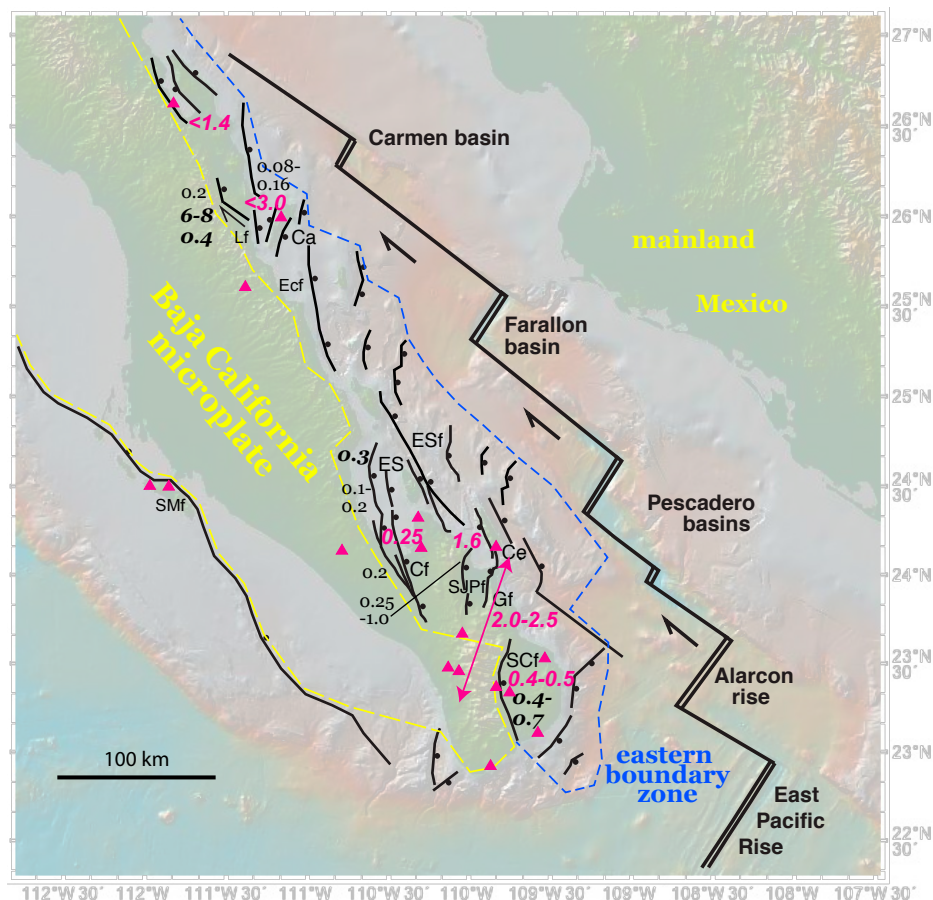
Figure 5. Map-based comparison of the faulting rates in mm/yr (km/m.y.) from long-term geologic data (large bold numbers), paleoseismology (smaller black numbers), and global positioning system (GPS; red numbers). See Figure 2 caption for abbreviations; see text for discussion.

to BCM motion, with the fault blocks moving northwest relative to North America (and the Pescadero and Farallon spreading centers), and parallel to the transform faults. At distances of ~45–60 km, this is a reasonable assumption if the fault locking depth is ~10 km. A similar locking depth was found for the Ballenas transform fault further north (Plattner et al., 2015) and may be adequate for the long transform segments in the Gulf of California. One would expect lower locking depths near the basins and seafloor spreading centers, which are more prominent in the south adjacent to the La Paz–Los Cabos region.

In contrast to the north, the southern part of the eastern boundary zone consistently shows east to northeast GPS-based motion relative to the BCM. The azimuth of these motions is both nearly perpendicular to the local active normal faults and toward the bathymetric deep of the axial gulf (Fig. 3). This strain pattern shows a significant degree of strain partitioning between the SW margin of the main southern Gulf of California and the strike-slip–dominated transform faults in the axial gulf. This conclusion agrees with earlier interpretations (Fletcher and Munguía, 2000; Dorsey and Umhoefer, 2012). Therefore, the southern part of the eastern boundary zone, south of 25°N, is currently highly strain partitioned, while the northern part shows no partitioning. The normal fault earthquakes of the past 50 yr confirm the high degree of active partitioning in the south (Fletcher and Munguía, 2000; Sumy et al., 2013). It is important to note that earthquakes in the study area have been analyzed over short periods of time (a few years), and mainly in the onshore to nearshore islands area (Munguía et al., 2006) and the axial gulf plate boundary (Sumy et al., 2013).

The active rates of motion along the eastern boundary zone of 2.5–3 mm/yr are minimum values because the GPS sites closest to the main plate boundary (WCAR and ECER) have known or likely active faults between each site and the axial gulf plate boundary. This means that the 50 mm/yr motion between the BCM and North America across the Alarcón spreading center (Fig. 2; Table 3) is distributed as >2.5 mm/yr across the southern part of the eastern boundary zone and <47.5 mm/yr on the adjacent Alarcón spreading center. Likewise, the 48.5–48.7 mm/yr motion between the BCM and North America across the Carmen and Farallon spreading centers is distributed as >3 mm/yr across the eastern boundary zone and <45.5–45.7 mm/yr on the spreading centers.

Comparison of Active to Short-Term and Long-Term Deformation

Similar to the active strain within the eastern boundary zone of the BCM, the comparison between the active to short-term (late Quaternary) and long-term (10⁶ yr) rates differs substantially in the north and the south. In the northern Loreto area, the Loreto fault and basin show long-term rifting rates of 0.4 mm/yr in the Pliocene before and after a short period of rapid faulting up to 6–8 mm/yr at ca. 2.4 Ma (Fig. 5; Dorsey and Umhoefer, 2000). Paleoseismology indicates that the northern Loreto fault and a fault offshore near the coast, 10–20 km north of the city of Loreto, each have late Quaternary faulting rates of 0.1–0.2 mm/yr (Fig. 5). The 3 mm/yr active motion of Carmen Island away from the BCM must be taking place on those two faults and the active faults in Loreto Bay between Loreto and Carmen Island shown by Nava-Sanchez et al. (2001). We can therefore conclude that the 3 mm/yr faulting rates across the northern area from the BCM to Carmen Island are mainly on the offshore faults in Loreto Bay. We can also conclude that there was a major fault reorganization and likely a significant slowing of faulting across the northern part of the eastern boundary zone since the rapid rate on the Loreto fault at 2.4 Ma. We suggest that change occurred when the Pescadero, Farallon, and Carmen spreading centers were initiated at 2–1 Ma.

In the southern area, the strain rates and high degree of strain partitioning observed in the current GPS data are similar to the results from both paleoseismologic and long-term geologic data (Fig. 5). A good example of this is the La Paz Bay area north of the city of La Paz (Figs. 2 and 6). The long-term faulting rates across La Paz Bay are 0.3 mm/yr, as summarized above, while the late Quaternary rates from multiple methods are 0.1–0.2 mm/yr (Umhoefer et al., 2014), and the GPS-derived rates from this study are 0.2–0.3 mm/yr. Also, GPS rates of 1.4 mm/yr are broadly similar across the San Juan de las Planes area, while the late Quaternary faulting rate on the fault on just the western side of the basin is 0.25–1.0 mm/yr (Busch et al., 2011). The San Jose del Cabo fault and basin area has long-term rates of 0.4–0.7 mm/yr since 12–10 Ma, which are the same as the 0.4–0.6 mm/yr GPS-derived rates across the fault. The motion from the CABO to RIVE GPS sites along the eastern coast of the peninsula is 1.1 ± 1.4 mm/yr.

Our study and the previous data on faulting from the late Quaternary and longer-term data summarized here lead to the following conclusions.

(1) Based mainly on GPS data from Carmen Island and previous work in the Loreto area, the northern part of the eastern boundary zone of the BCM is linked to the main gulf-axis plate boundary as a broad zone of northwesterly moving transtensional deformation.

(2) The southern La Paz to Cabo San Lucas area shows a high degree of strain partitioning in all data sets across time, supporting previous conclusions (Fletcher and Munguía, 2000; Dorsey and Umhoefer, 2012) that NE to ENE extension there is markedly different than the northwestward motion along the gulf-axis plate boundary. The eastern boundary zone of the BCM onshore and in the near offshore has a remarkable consistency of normal faulting since 12 Ma on individual faults from current GPS to long-term geologic data, most notably on the Carrizal and San Jose del Cabo faults (Fig. 5).

(3) The La Paz latitude transect across the widest part of the eastern boundary zone shows that the faults farther offshore have higher rates of active (and older) faulting than those along the rift escarpment (Figs. 3 and 6). This result is similar to the conclusions from the Loreto area transect from the rift escarpment (Loreto fault) to Carmen Island.

(4) The >2.5–>3 mm/yr motion across the eastern boundary zone in the north and south suggests that at least 5%–6% of the 48.5–50 mm/yr BCM to North America relative motion is within the northern transtensional zone and southern strain-partitioned zone, while 95%–94% of the relative motion is occurring at the offshore spreading centers. The 5%–6% range is a minimum because there are proven or likely active faults between the easternmost GPS sites and the main axial plate boundary.

Mechanisms for Continued Rifting While Drifting

Our results suggest these important questions for the process of rupturing of a continent by oblique rifting. Why is rifting (faulting) continuing 3–6 m.y. after seafloor spreading initiated in the southern Gulf of California, contradicting the rift-to-drift hypothesis? Why does rifting continue during drifting
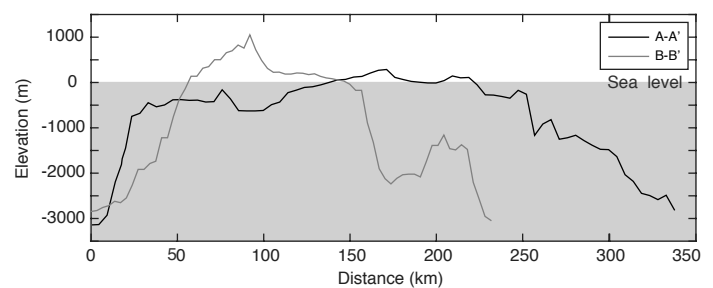
Figure 6. Topographic gradient along transects A-A′ and B-B′ as shown in Figure 3.

only on the western side of the gulf? What is driving the active tectonics of the eastern boundary zone of the BCM in the southern Gulf of California? We do not have concrete answers for these questions, but we discuss possible mechanisms here. While we analyzed the kinematics from the GPS data and discussed the motion azimuths in relation to the local fault network and topographic gradients, we cannot quantitatively distinguish between gravitational or plate-tectonic driving forces. Attempts to use mechanical models to decipher between the two mechanisms are beyond the scope of this paper.

We speculate that the main mechanism for active faulting is potential energy as an added force on the tectonic faults driven by the large relief between the high rift escarpment on the Baja California Peninsula and the deep axial Gulf of California (Figs. 2 and 6). The relief was inherited from the much faster faulting of the BCM boundary before plate motions localized along the modern transform–spreading centers as summarized here. The hypothesis is that the 3–4.5 km difference in elevation between the 1–1.5 km elevation rift escarpment along the eastern side of the Baja California Peninsula (and eastern edge of the BCM; Fig. 2) and the deep gulf-axis basins 2–3 km below sea level creates a significant gradient in the gravitational potential energy that drives a continuation of deep-seated tectonic faulting. In essence, we are arguing that the long-term, east-dipping tectonic faults (northern Loreto, Carrizal, San Juan de las Planes, and San Jose del Cabo faults) have become hybrid tectonic-gravity–driven faults. That is, the faulting remains characterized by typical normal fault earthquakes, but the potential energy of the relief across the margin is prolonging this activity.

This topographic gradient occurs across a zone of numerous faults that are now active at <1 to ~2 mm/yr rates. As summarized here, these rates are significantly lower than faulting rates in the past in the north near Loreto, and about the same as past rates in the south. Transect B-B′ across the topographic gradient discussed here shows a rapid decrease in elevation at the rift escarpment, and then another large change in relief in the eastern coastal area to near offshore, and then another rapid decay in elevation farther offshore down to 2500–3500 m below sea level in the deep basins. Topographic transects across the eastern boundary zone farther north would have a wider offshore area but the same general pattern. These steeper slopes are the location of active strain localizing on the preexisting normal faults. The deeper offshore region appears to be largely inactive (Sutherland et al., 2012), but earthquakes in the past 20 yr demonstrate that major parts of the offshore eastern boundary zone remain seismically active.

The second set of factors that we argue contribute to the rifting while drifting process is related to the generally arid climate of the southern Baja California Peninsula and islands. The late Quaternary to active faulting, even at relatively slow rates, maintains relatively high topographic relief over millions of years in this region. The low sediment flux from the small drainages on the southern Baja California Peninsula and the semiarid to arid climate result in relatively low erosion rates and underfilled basins (Dorsey and Umhoefer, 2012; Sutherland et al., 2012). We suggest that the surficial processes under these conditions allow the high relief and large elevation gradient to persist over geologic time scales. This is in contrast to the eastern side of the gulf, where the basins are filled (Fig. 1) and faulting ceased approximately at 6–3 Ma when seafloor spreading began (Sutherland et al., 2012).

The eastern boundary zone of the BCM is mainly present from Bahia Concepcion to Loreto to the south in a southward-widening zone (Fig. 2). Few active faults lie along the plate boundary north of there until northern Baja California. The location of the zone of active faulting is spatially coincident with the western margin of the Alarcón to Farallon rift domains or the western side of the south-central domain of Lizarralde et al. (2007; see also Fig. 1 herein). The Alarcón rift domain is a wide rift that had ~350 km of extension before seafloor spreading on the Pescadero, Farallon, and Carmen basins at 3–2 Ma. Lizarralde et al. (2007) observed from

seismic refraction data and previous studies onshore that the rifting had little accompanying magmatism. Furthermore, they suggested that the south-central domain was underlain by strong lithospheric mantle that did not readily melt due to its location over the previous early Miocene ignimbrite belt (Ferrari et al., 2007), which left the mantle depleted. The eastern boundary zone of the BCM of this study was inherited from the wide rift margin of the south-central domain, and its wedge-like shape may have a control on strain partitioning (Fig. 2).

That leads to the final aspect of the study area we address: the vastly different degrees of strain partitioning from none in the north to a high degree in the south. One simple explanation may be the variable width of the eastern boundary zone. From 25°N and north, the rift escarpment to main plate boundary is ~30–75 km wide, while from 25°N and south, that width is from 75–120 km. The no-strain-partitioning area in the north near and offshore of Loreto has similarities to a narrow transtensional belt to the southeast toward the Pescadero and Alarcón spreading centers (Fig. 2). The seismic reflection line described by Sutherland et al. (2012) includes some basins that have transtensional instead of merely normal fault traits, and many faults mapped from bathymetry have northwest- to north-striking kinks, much like the well-understood transtensional Loreto and San Jose Island faults (Dorsey and Umhoefer, 2000; Umhoefer et al., 2007). In contrast, the highly strain partitioned zone described above in the La Paz to Cabo San Lucas area may be confined to the normal faults from the rift escarpment to the offshore fault on the eastern side of Cerralvo Island (Fig. 2).

REFERENCES CITED

Amos, C.B., Audet, P., Hammond, W.C., Burgmann, R., Johanson, I.A., and Blewitt, G., 2014, Uplift and seismicity driven by groundwater depletion in central California: Nature, v. 509, p. 483–486, https://doi.org/10.1038/nature13275.

Bennett, R.A., Wernicke, B.P., Niemi, N.A., and Friedrich, A.M., 2003, Contemporary strain rates in the northern Basin and Range province from GPS data: Tectonics, v. 22, https://doi.org/10.1029/2001TC001355.

Bennett, S.E.K., Oskin, M.E., and Iriondo, A., 2013, Transtensional rifting in the proto–Gulf of California, near Bahia Kino, Sonora, Mexico: Geological Society of America Bulletin, v. 125, p. 1752–1782, https://doi.org/10.1130/B30676.1.

Brothers, D., Harding, A., González-Fernández, A., Holbrook, W.S., Kent, G., Driscoll, N., Fletcher, J., Lizarralde, D., Umhoefer, P.J., and Axen, G., 2012, Farallon slab detachment and deformation of the Magdalena Shelf, southern Baja California: Geophysical Research Letters, v. 39, L09307, https://doi.org/10.1029/2011GL050828.

Busch, M.M., Arrowsmith, J.R., Umhoefer, P.J., Coyan, J.A., Maloney, S., and Martínez Gutiérrez, G., 2011, Geometry and evolution of rift-margin, normal-fault bounded basins from gravity and geology, La Paz–Los Cabos region, Baja California Sur, Mexico: Lithosphere, v. 3, p. 110–127, https://doi.org/10.1130/L113.1.

Chamoli, A., Lowry, A.R., and Jeppson, T.N., 2014, Implications of transient deformation in the northern Basin and Range, western United States: Journal of Geophysical Research–Solid Earth, v. 119, p. 4393–4413, https://doi.org/10.1002/2013JB010605.

Coyan, M.M., Arrowsmith, J.R., Umhoefer, P.J., Coyan, J.A., Kent, G., Driscoll, N., and Martínez-Gutiérrez, G., 2013, Geometry and Quaternary slip behavior of the San Juan de los Planes and Saltito fault zones, Baja California Sur, Mexico: Characterization of rift margin normal faults: Geosphere, v. 9, p. 426–443, https://doi.org/10.1130/GES00806.1.

DeMets, C., 1995, Reappraisal of seafloor spreading lineations in the Gulf of California: Implications for the transfer of Baja California to the Pacific plate and estimates of Pacific–North America motion: Geophysical Research Letters, v. 22, p. 3545–3548, https://doi.org/10.1029/95GL03323.

DeMets, C., Gordon, R.G., Argus, D.F., and Stein, S., 1990, Current plate motions: Geophysical Journal International, v. 101, p. 425–478, https://doi.org/10.1111/j.1365-246X.1990.tb06579.x.

DeMets, C., Gordon, R.G., Argus, D.F., and Stein, S., 1994, Effect of recent revisions to the geomagnetic reversal time-scale on estimates of current plate motions: Geophysical Research Letters, v. 21, p. 2191–2194, https://doi.org/10.1029/94GL02118.

DeMets, C., Gordon, R.G., and Argus, D.F., 2010, Geologically current plate motions: Geophysical Journal International, v. 181, p. 1–80, https://doi.org/10.1111/j.1365-246X.2009.04491.x.

Dixon, T., Farina, F., DeMets, C., Suarez-Vidal, F., Fletcher, J., Marquez-Azua, B., Miller, M., Sanchez, O., and Umhoefer, P., 2000, New kinematic models for Pacific-North America motion from 3 Ma to present: Evidence for a "Baja California shear zone": Geophysical Research Letters, v. 27, p. 3961–3964, https://doi.org/10.1029/2000GL008529.

Dorsey, R.J., and Umhoefer, P.J., 2000, Tectonic and eustatic controls on sequence stratigraphy of the Pliocene Loreto basin, Mexico: Geological Society of America Bulletin, v. 112, p. 177–199, https://doi.org/10.1130/0016-7606(2000)112<177:TAECOS>2.0.CO;2.

Dorsey, R.J., and Umhoefer, P.J., 2012, Influence of sediment input and plate-motion obliquity on basin development along an active oblique divergent plate boundary: Gulf of California and Salton Trough, in Busby, C.J., and Azor, A., eds., Tectonics of Sedimentary Basins: Recent Advances: Oxford, UK, Wiley-Blackwell Publishing, p. 209–225, https://doi.org/10.1002/9781444347166.ch10.

Efron, B., 1979, Bootstrap methods: Another look at the Jackknife: Annals of Statistics, v. 7, p. 1–26, https://doi.org/10.1214/aos/1176344552.

Ferrari, L., López-Martínez, M., and Rosas-Elguera, J., 2002, Ignimbrite flare-up and deformation in the southern Sierra Madre Occidental, western Mexico: Implications for the late subduction history of the Farallon plate: Tectonics, v. 21, p. 17-1–17-24, https://doi.org/10.1029/2001TC001302.

Ferrari, L., Valencia-Moreno, M., and Bryan, S., 2007, Magmatism and tectonics of the Sierra Madre Occidental and its relation with the evolution of the western margin of North America, in Alaniz-Álvarez, S.A., and Nieto-Samaniego, Á.F., eds., Geology of México: Celebrating the Centenary of the Geological Society of México: Geological Society of America Special Paper 422, p. 1–39, https://doi.org/10.1130/2007.2422(01).

Ferrari, L., López-Martínez, M., Orozco-Esquivel, T., Bryan, S.E., Duque-Trujillo, J., Lonsdale, P., and Solari, L., 2013, Late Oligocene to middle Miocene rifting and synextensional magmatism in the southwestern Sierra Madre Occidental, Mexico: The beginning of the Gulf of California rift: Geosphere, v. 9, p. 1161–1200, https://doi.org/10.1130/GES00925.1.

Fletcher, J.M., and Munguía, L., 2000, Active continental rifting in southern Baja California, Mexico: Implications for plate motion partitioning and the transition to seafloor spreading in the Gulf of California: Tectonics, v. 19, p. 1107–1123, https://doi.org/10.1029/1999TC001131.

Fletcher, J.M., Kohn, B.P., Foster, D.A., and Gleadow, A.J.W., 2000, Heterogeneous Neogene cooling and exhumation of the Los Cabos block, southern Baja California: Evidence from fission-track thermochronology: Geology, v. 28, p. 107–110, https://doi.org/10.1130/0091-7613(2000)28<107:HNCAEO>2.0.CO;2.

Friedrich, A.M., Lee, J., Wernicke, B.P., and Sieh, K., 2004, Geologic context of geodetic data across a Basin and Range normal fault, Crescent Valley, Nevada: Tectonics, v. 23, TC2015, https://doi.org/10.1029/2003TC001528.

Fu, Y., Argus, D.F., and Landerer, F.W., 2015, GPS as an independent measurement to estimate terrestrial water storage variations in Washington and Oregon: Journal of Geophysical Research–Solid Earth, v. 120, p. 552–566, https://doi.org/10.1002/2014JB011415.

Goff, J.A., Bergman, E.A., and Solomon, S.C., 1987, Earthquake source mechanisms and transform fault tectonics in the Gulf of California: Journal of Geophysical Research, v. 92, p. 10485–10510, https://doi.org/10.1029/JB092iB10p10485.

Hackl, M., Malservisi, R., Hugentobler, U., and Wonnacott, R., 2011, Estimation of velocity uncertainties from GPS time series: Examples from the analysis of the South African Trignet network: Journal of Geophysical Research, v. 116, B11404, https://doi.org/10.1029/2010JB008142.

Hackl, M., Malservisi, R., Hugentobler, U., and Jiang, Y., 2013, Velocity covariance in the presence of anisotropic time correlated noise and transient events in GPS time series: Journal of Geodynamics, v. 72, p. 36–45, https://doi.org/10.1016/j.jog.2013.08.007.

Heezen, B.C., 1969, The world rift system: An introduction to the symposium: Tectonophysics, v. 8, p. 269–279, https://doi.org/10.1016/0040-1951(69)90037-7.

Johnson, M.E., Ledesma-Vázquez, J., and Backus, D.H., 2016, Tectonic decapitation of a Pliocene mega-delta on Isla del Carmen in the Gulf of California (Mexico): And a river ran through it: The Journal of Geology, v. 124, p. 55–74, https://doi.org/10.1086/684206.

Kreemer, C., Blewitt, G., and Klein, E.C., 2014, A geodetic plate motion and global strain rate model: Geochemistry, Geophysics, Geosystems, v. 15, p. 3849–3889, https://doi.org/10.1002/2014GC005407.

Kreemer, C., Hammond, W.C., and Blewitt, G., 2018, A robust estimation of the 3D intraplate deformation of the North American plate from GPS: Journal of Geophysical Research–Solid Earth, v. 123, p. 4388–4412, https://doi.org/10.1029/2017JB015257.

Ledesma-Vazquez, J., and Johnson, M.E., 2001, Miocene–Pleistocene tectono-sedimentary evolution of Bahia Concepcion region, Baja California Sur (Mexico): Sedimentary Geology, v. 144, p. 83–96, https://doi.org/10.1016/S0037-0738(01)00136-1.

Le Pichon, X., 1968, Sea-floor spreading and continental drift: Journal of Geophysical Research, v. 73, p. 3661–3697, https://doi.org/10.1029/JB073i012p03661.

Lizarralde, D., Axen, G.J., Brown, H.E., Fletcher, J.M., González-Fernández, A., Harding, A.J., Holbrook, W.S., Kent, G.M., Paramo, P., Sutherland, F., and Umhoefer, P.J., 2007, Variable styles of rifting in the Gulf of California: Nature, v. 448, p. 466–469, https://doi.org/10.1038/nature06035.

Lonsdale, P., 1989, Geology and tectonic history of the Gulf of California, in Winterer, E.L., et al., eds., The Eastern Pacific Ocean and Hawaii: Boulder, Colorado, Geological Society of America, Geology of North America, v. N, p. 499–521.

Lonsdale, P., 1991, Structural patterns of the Pacific floor offshore of Peninsular California, in Dauphin, J.P., and Simoneit, B.T., eds., Gulf and Peninsula Province of the Californias: American Association of Petroleum Geologists Memoir 47, p. 87–125.

Lucazeau, F., Leroy, S., Autin, J., Bonneville, A., Goutorbe, B., Watremez, L., d'Acremont, E., Dusunur, D., Rolandone, F., Huchon, P., Bellahsen, N., and Tuchais, P., 2009, Post-rift volcanism and high heat-flow at the ocean-continent transition of the eastern Gulf of Aden: Terra Nova, v. 21, p. 285–292, https://doi.org/10.1111/j.1365-3121.2009.00883.x.

Macy, J., 2005, Rotation and Uplift of Carmen Island, Baja California Sur, Mexico [M.S. thesis]: Flagstaff, Arizona, Northern Arizona University, 126 p.

Malservisi, R., Schwartz, S.Y., Voss, N., Protti, M., Gonzalez, V., Dixon, T.H., Jiang, Y., Newman, A.V., Richardson, J., Walter, J.I., and Voyenko, D., 2015, Multiscale post seismic behavior on a megathrust: The 2012 Nicoya earthquake, Costa Rica: Geochemistry Geophysics Geosystems, v. 16, p. 1848–1864, https://doi.org/10.1002/2015GC005794.

Mao, A., Harrison, G.A., and Dixon, T.H., 1999, Noise in GPS coordinate time series: Journal of Geophysical Research–Solid Earth, v. 104, p. 2797–2816, https://doi.org/10.1029/1998JB900033.

Masson, D.G., Cartwright, J.A., Pinheiro, L.M., Whitmarsh, R.B., Beslier, M.O., and Roeser, H., 1994, Compressional deformation at the ocean-continent transition in the NE Atlantic: Journal of the Geological Society [London], v. 151, p. 607–613, https://doi.org/10.1144/gsjgs.151.4.0607.

Mayer, L., and Vincent, K.R., 1999, Active tectonics of the Loreto area, Baja California Sur, México: Geomorphology, v. 27, p. 243–255, https://doi.org/10.1016/S0169-555X(98)00074-9.

Mohriak, W.U., and Leroy, S., 2013, Architecture of rifted continental margins and break-up evolution: Insights from the South Atlantic, North Atlantic and Red Sea–Gulf of Aden conjugate margins, in Mohriak, W.U., et al., eds., Conjugate Divergent Margins: Geological Society [London] Special Publication 369, p. 497–535, https://doi.org/10.1144/SP369.17.

Munguía, L., Gonzalez, M., Mayer, S., and Aguirre, A., 2006, Seismicity and state of stress in the La Paz–Los Cabos region, Baja California Sur, Mexico: Bulletin of the Seismological Society of America, v. 96, p. 624–636, https://doi.org/10.1785/0120050114.

Nava-Sanchez, E.H., Gorsline, D.S., and Molina-Cruz, A., 2001, The Baja California Peninsula borderland: Structural and sedimentological characteristics: Sedimentary Geology, v. 144, p. 63–82, https://doi.org/10.1016/S0037-0738(01)00135-X.

Peron-Pinvidic, G., Shillington, D., and Tucholke, B., 2010, Characterization of sills associated with the U reflection on the Newfoundland margin: Evidence for widespread early post-rift magmatism on a magma-poor rifted margin: Geophysical Journal International, v. 182, p. 113–136.

Peron-Pinvidic, G., Manatschal, G., and Osmundsen, P.T., 2013, Structural comparison of archetypal Atlantic rifted margins: A review of observations and concepts: Marine and Petroleum Geology, v. 43, p. 21–47, https://doi.org/10.1016/j.marpetgeo.2013.02.002.

Plattner, C., Malservisi, R., Dixon, T.H., LaFemina, P., Sella, G.F., Fletcher, J., and Suarez-Vidal, F., 2007, New constraints on relative motion between the Pacific plate and Baja California microplate (Mexico) from GPS measurements: Geophysical Journal International, v. 170, p. 1373–1380, https://doi.org/10.1111/j.1365-246X.2007.03494.x.

Plattner, C., Malservisi, R., Amelung, F., Dixon, T.H., Hackl, M., Verdecchia, A., Lonsdale, P., Suarez-Vidal, F., and Gonzalez-Garcia, J., 2015, Space geodetic observation of the deformation cycle across the Ballenas transform, Gulf of California: Journal of Geophysical Research–Solid Earth, v. 120, p. 5843–5862, https://doi.org/10.1002/2015JB011908.

Puchalski, M.C., 2002, Style, Kinematics, and Timing of Major Faults on Isla Espiritu Santo, Baja California Sur, Mexico [M.S. thesis]: Flagstaff, Arizona, Northern Arizona University, 166 p.

Rebischung, P., Griffiths, J., Ray, J., Schmid, R., Colilieux, X., and Garayt, B., 2012, IGS08: The IGS realization of the ITRF2008: GPS Solutions, v. 16, p. 483–494, https://doi.org/10.1007/s10291-011-0248-2.

Shillington, D.J., Hopper, J.R., and Holbrook, W.S., 2008, Seismic signal penetration beneath post-rift sills on the Newfoundland rifted margin: Geophysics, v. 73, p. B99–B107, https://doi.org/10.1190/1.2972131.

Stein, S., and Gordon, R.G., 1984, Statistical tests of additional plate boundaries from plate motion inversions: Earth and Planetary Science Letters, v. 69, p. 401–412, https://doi.org/10.1016/0012-821X(84)90198-5.

Sumy, D., Gaherty, J.B., Kim, W.-Y., Diehl, T., and Collins, J., 2013, The mechanisms of earthquakes and faulting in the southern Gulf of California: Bulletin of the Seismological Society of America, v. 103, p. 487–506, https://doi.org/10.1785/0120120080.

Sutherland, F.H., Kent, G.M., Harding, A.J., Umhoefer, P.J., Driscoll, N.W., Lizarralde, D., Fletcher, J.M., Axen, G.J., Holbrook, W.S., González-Fernández, A., and Lonsdale, P., 2012, Middle Miocene to early Pliocene oblique extension in the southern Gulf of California: Geosphere, v. 8, p. 752–770, https://doi.org/10.1130/GES00770.1.

Umhoefer, P.J., 2011, Why did the southern Gulf of California rupture so rapidly?—Oblique divergence across hot, weak lithosphere along a tectonically active margin: GSA Today, v. 21, p. 4–10, https://doi.org/10.1130/G133A.1.

Umhoefer, P.J., Mayer, L., and Dorsey, R.J., 2002, Evolution of the margin of the Gulf of California near Loreto, Baja California Peninsula, Mexico: Geological Society of America Bulletin, v. 114, p. 849–868, https://doi.org/10.1130/0016-7606(2002)114<0849:EOTMOT>2.0.CO;2.

Umhoefer, P.J., Schwenicke, T., Del Margo, M.T., Ruiz-Geraldo, G., Ingle, J.C., Jr., and McIntosh, W., 2007, Transtensional fault-termination basins: An important basin type illustrated by the Pliocene San Jose Island basin and related basins in the southern Gulf of California, Mexico: Basin Research, v. 19, p. 297–322, https://doi.org/10.1111/j.1365-2117.2007.00323.x.

Umhoefer, P.J., Maloney, S.J., Buchanan, B., Arrowsmith, J.R., Martinez-Gutiérrez, G., Kent, G., Driscoll, N., Harding, A., Kaufman, D., and Rittenour, T., 2014, Late Quaternary faulting history of the Carrizal and related faults, La Paz region, Baja California Sur, Mexico: Geosphere, v. 10, p. 476–504, https://doi.org/10.1130/GES00924.1.

Wernicke, B.P., and Davis, J.L., 2010, Detecting large-scale intracontinental slow-slip events (SSEs) using geodograms: Seismological Research Letters, v. 81, p. 694–698, https://doi.org/10.1785/gssrl.81.5.694.

Wetmore, P.H., Malservisi, R., Fletcher, J.M., Alsleben, H., Wilson, J., Callihan, S., Springer, A., Gonzales-Yajimovich, O., and Gold, P.O., 2019, Slip history and the role of the Agua Blanca fault in the tectonics of the North American–Pacific plate boundary of southern California, USA, and Baja California, Mexico: Geosphere, v. 15, p. 119–145, https://doi.org/10.1130/GES01670.1.

Zumberge, J.F., Heflin, M.B., Jefferson, D.J., Watkins, M.M., and Webb, F.H., 1997, Precise point positioning for the efficient and robust analysis of GPS data from large networks: Journal of Geophysical Research–Solid Earth, v. 102, p. 5005–5017, https://doi.org/10.1029/96JB03860.